Numerical and experimental investigations for the evaluation of the wear coefficient of reverse total shoulder prostheses

Lorenza Mattei[1*], Francesca Di Puccio[1], Thomas J. Joyce[2], Enrico Ciulli[1]

[1]Department of Civil and Industrial Engineering, Largo Lucio Lazzarino 2, Pisa, 56126, IT

[2]School of Mechanical and Systems Engineering, Stephenson Building, Claremont Road, Newcastle upon Tyne, NE1 7RU, UK

Abstract

In the present study, numerical and experimental wear investigations on reverse total shoulder arthroplasties (RTSAs) were combined in order to estimate specific wear coefficients, currently not available in the literature. A wear model previously developed by the authors for metal-on-plastic hip implants was adapted to RTSAs and applied in a double direction: firstly, to evaluate specific wear coefficients for RTSAs from experimental results and secondly, to predict wear distribution. In both cases, the Archard wear law (AR) and the wear law of UHMWPE (PE) were considered, assuming four different *k* functions. The results indicated that both the wear laws predict higher wear coefficients for RTSA with respect to hip implants, particularly the AR law, with *k* values higher than twofold the hip ones. Such differences can significantly affect predictive wear model results for RTSA, when non-specific wear coefficients are used. Moreover, the wear maps simulated with the two laws are markedly different, although providing the same wear volume. A higher wear depth (+51%) is obtained with the AR law, located at the dome of the cup, while with the PE law the most worn region is close to the edge. Taking advantage of the linear trend of experimental volume losses, the wear coefficients obtained with the AR law should be valid despite having neglected the geometry update in the model.

Keywords: reverse total shoulder arthroplasty, wear law, wear coefficient, cross-shear, wear modelling, in vitro wear tests.

1 Introduction

Reverse total shoulder arthroplasty (RTSA) is considered the gold standard to treat rotator cuff tear arthropathy (Fig.1.a). It is also used to revise failed anatomical total shoulder arthroplasties (ATSAs) and to treat proximal humeral tumours and fractures. RTSA is performed by replacing the humeral head and the glenoid cavity with a plastic cup in ultra high molecular weight polyethylene (UHMWPE) and a metallic head respectively (Fig.1.b), in a geometrical reversed configuration with respect to the anatomical one. First introduced in the 1970s, RTSA has become popular only recently, thanks to the modern Grammont design (Boileau et al., 2005) and its FDA approval in 2003. The Grammont design is characterized by a large glenoid head, without neck, and a humeral cup with an almost vertical axis that allows, respectively, i) a medialization of the centre of rotation, which helps to minimize the torque at the glenoid component-bone interface and to recruit more deltoid fibers, ii) a lowered position of the humerus with respect to the acromion, which restores and increases the deltoid tension. As a consequence, the modern reverse design results in iii) a wider range of motion (up to 90° of abduction) and a more stable implant.

*Corresponding author: l.mattei@ing.unipi.it; (+39)3492506500

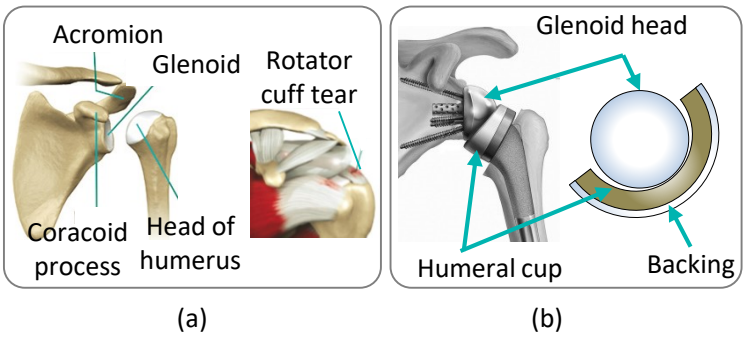

Fig.1. Shoulder anatomy and rotator cuff tear (a). Reverse shoulder implant and model geometry (b).

Although clinical outcomes are encouraging, the rate of complications and revisions is high, probably because the reverse design significantly alters the biomechanics of the natural shoulder joint. According to the literature, the most common complication is the inferior-posterior scapular notching, with an incidence of 0% to 100%, whilst the main cause of revision is glenoid loosening with an incidence up to 10% (Boileau et al., 2005; Farshad and Gerber, 2010; Nam et al., 2010; Wiater et al., 2014). It is widely recognised that notching is seen in explanted reverse shoulder implants (Nam et al., 2010; Nyffeler et al., 2004; Kohut et al., 2012) and that such notching can be a cause of substantial amounts of polyethylene wear debris. Further, this mechanical impingement puts the fixation at greater risk due to removal of supporting bone under the glenoid component. However it has been suggested that scapular notching may be made worse by wear debris from the articulating surfaces (Vaupel et al., 2012). It is also recognised that notching may be reduced by modifications to implant designs (Chou et al., 2009; Kohut et al., 2012) and optimal positioning of components. Therefore it is important to understand and determine the wear due to 'normal' articulation in reverse shoulder prostheses so that a baseline can be established (Smith et al., 2015).

In comparison to hip and knee implants, wear in shoulder prostheses has not been thoroughly investigated. Indeed, no wear test standards exist and there are very few shoulder simulators. Likely this is due to the extreme complexity of the shoulder joint and to the wide variety of daily shoulder movements. Consequently, only a few experimental investigations on wear of RTSA can be found in the literature (Kohut et al., 2012; Peers et al., 2015; Smith et al., 2013), which simulate different (and hardly comparable) working conditions. For instance, loading and motion profiles tested in (Kohut et al., 2012) are adapted from ISO 14242 for hip implants , whilst (Peers et al., 2015; Vaupel et al., 2012) simulate alternating cycles of flexion and abduction.

Numerical wear investigations on RTSA are restricted to a few studies (Quental et al., 2015; Ribeiro et al., 2011; Terrier et al., 2009), which are mainly focused on the comparison between anatomical and reverse solutions and often simplified in terms of simulated conditions (e.g. unloaded abduction-adduction) and wear law (e.g. Archard law with a constant wear coefficient) (Ribeiro et al., 2011; Terrier et al., 2009). Indeed, only in (Quental et al., 2015) the fundamental cross-shearing effect of the UHMWPE wear is considered assuming the new formulation of the wear law for UHMWPE recently proposed by Liu et al.(Liu et al., 2011). Actually, the main limit of all such wear models lies in the values/expressions assumed for the wear coefficient k, since they were originally estimated for hip (Maxian et al., 1997; Saikko, 2006) and knee (Abdelgaied et al., 2011) implants. In fact, as is well known, the wear coefficient does not depend only on the material coupling but is also notably affected by the implant geometry, the loading/kinematic conditions and the lubrication regime. Consequently, k should be considered as a very specific quantity, which can be estimated by means of experimental and numerical wear simulations reproducing the effective working conditions (Di Puccio and Mattei, 2015a). Therefore, the use in wear modelling of RTSA of a value for k derived for hip/knee implants can compromise the reliability of wear simulations. On the other hand, to the best of authors' knowledge, wear coefficients of RTSA components are not available in the literature.

The main purpose of the present study is to evaluate reliable wear coefficients for RTSAs by means of numerical and experimental investigations, which are useful to characterize and compare RTSA designs, and

as input data for numerical wear simulations. An experimental wear test on 42 mm diameter RTSA samples was carried out using a recently developed multi-station shoulder wear simulator (Smith et al., 2013). The test was then numerically simulated using an analytical wear model presented in (Mattei et al., 2013) and here adapted to shoulder implants. In particular, two wear laws were simulated. These were the Archard law and one for the wear of UHMWPE. In each case different expressions of the wear factor k were considered, also including the cross-shear effect. The comparison of experimental and numerical wear volumes allowed several wear coefficients for the examined RTSA to be estimated, which is innovative with respect to the literature.

2 Materials and Methods

2.1 Experimental wear investigation

A 2 million cycle wear test was performed with JRI Orthopaedics Reverse VAIOS shoulder prostheses (Smith et al., 2013) using a recently developed multi-station shoulder wear simulator, presented in (Smith et al., 2015). The test group consisted in five shoulder prostheses each with a 42.1 mm diameter UHMWPE cup and an average diametrical clearance of 0.14 mm. Figure 2 shows some of these components with the metallic glenosphere shown on the far right of the image and the UHMWPE humeral component on its immediate left. Also indicated is where the UHMWPE component fits inside its test bath. An additional sixth prosthesis was subjected to dynamic loading, but no motion, in the 'control' station thus allowing the influence of lubricant uptake by the UHMWPE components to be taken into account.

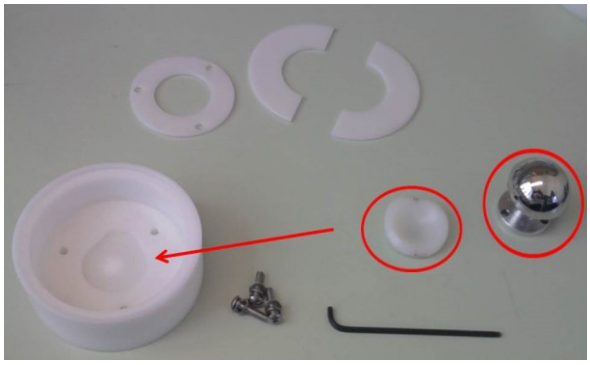

Fig.2. A sample test prosthesis.

Figure 3 shows an overview of the simulator. The test baths have been removed for clarity, but to the left the bronze coloured test bath mounting can be seen. Also visible are two of the pneumatic cylinders that provided two of the motions to test components. Indeed, the simulator can apply two orthogonal rotations to the unloaded components. They correspond to the flexion-extension (FE) and the abduction-adduction (AA) rotations, applied in the sequence FE->AA, whose axis mechanisms are visible in Fig.3, coloured in red and blue, respectively. A third rotation, corresponding to the inward-outward (IO) rotation, is applied to the loaded component. In particular, the load is applied along the axis of the IO rotation, i.e. in vertical direction. In Fig.3, the bronze coloured components form part of IO axis. In the present test, as summarized in Fig.4a, FE and AA rotations were applied to the head (glenosphere), whilst the IO rotation and the load were applied to the cup.

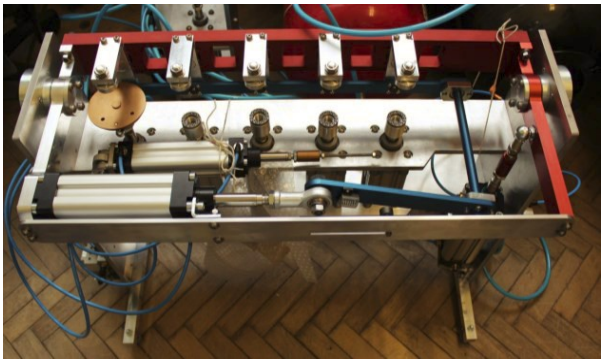

Fig.3. Experimental set up.

Testing ran to two million cycles under loading and motion conditions applicable to a person lifting a cup to their mouth or 'mug to mouth' as the activity of daily living was called. Motion and loading are shown in Figs.4b and 4c, respectively (Kontaxis, 2010). During a cycle of period *T* of 1 s, the load ranged between 180 N and 250 N, while FE, AA and IO angles respectively between -12°–16°, 5°–18° and -42°–17°.

Testing took place in a lubricant of dilute (50%) newborn calf serum (Sigma Aldrich n4637), giving an average protein content of 26 g/l, at ambient temperature.

Gravimetric measurements (Denver Instruments TB-215D, sensitivity 10μg) at intervals over the course of testing were used to determine the polymeric wear. The cleaning and weighting procedures employed were based on ISO 14242-2 for testing hip prostheses, in the absence of a similar ISO protocol for shoulder prostheses. Weight change was then converted to a volume using a density for the not cross-linked UHMWPE of 938 kg/m^3.

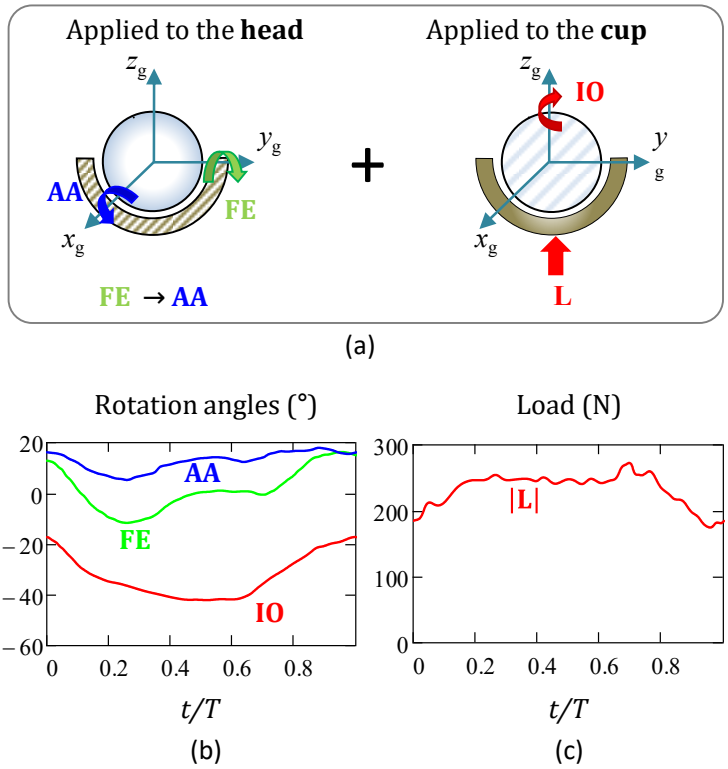

Fig.4. Simulated working conditions. Application of rotations and load to the head and cup (a). Time variation of rotation angles (b) and load (c) during a mug-to-mouth task (Kontaxis, 2010). Legend: FE: Flexion-Extension; AA: Abduction-Adduction; IO: inward-outward rotation.

2.2 Numerical wear model

The analytical wear model for metal-on-plastic hip replacements presented in (Mattei et al., 2013) was modified and adapted to total shoulder arthroplasty (TSA), for both anatomical (ATSA) and reverse configurations. Indeed, shoulder implants have the same ball-in-socket geometry and bearing materials used in hip prostheses. The characteristics of the new model are briefly described in the following, mainly focusing on the innovative aspects. The latter allowed obtaining a more versatile simulation tool capable of dealing with the kinematics and contact aspects of ball-in-socket implants with different conformity.

First of all, in the case of low conformal coupling such as the ATSAs (radial mismatch up to 10 mm), the head and cup centres cannot be considered coincident as assumed for hip implants in (Mattei et al., 2013), but their relative motion must be taken in account. Secondly, whilst in (Mattei et al., 2013), a finite element approach was used for contact analysis, here, a purely analytical formulation is proposed, based on Bartel's formulas (Bartel et al., 1985). Such formulas, reported in the Appendix, have been preliminarily validated with respect to finite element solutions (the difference was lower than 2%).

2.2.1 Model assumptions

The proposed model is based on some basic assumptions that allowed the implementation to be simplified and the computational costs reduced. In particular:

1. The geometry variation due to wear does not affect the contact mechanics.
2. The (metallic) head wear is negligible with respect to the wear of the plastic cup.
3. The effect of friction (usually lower than 0.065 (Brockett et al., 2007)) on contact pressure is negligible, as proved in (Liu et al., 2003).
4. The elastic deformation is negligible in kinematic analysis, i.e. in the evaluation of the coordinates and sliding velocity of a surface cup point.
5. The creep effects are negligible.

It is worth observing that the first hypothesis entails that wear predictions hold only for the initial phase of the wear process, when the effect of the geometry update is negligible (Kohut et al., 2012; Peers et al., 2015; Smith et al., 2013; Vaupel et al., 2012). However, as wear progresses, the geometry update is necessary, as shown in (Quental et al., 2015).

Further hypotheses are needed for the contact analysis, according to Bartel et al. (Bartel et al., 1985) (see Appendix A).

2.2.2 Wear laws

According to the literature, the wear laws currently used for describing UHMWPE-metal wear are two: the traditional Archard's wear law and a recent one specifically proposed for UHMWPE-metal couples in (Liu et al., 2011). Both wear laws were considered in the present study, referred to as AR and PE law, respectively. In particular, the PE law allows some important experimental observations on UHMWPE-metal wear to be taken into account, i.e. that the UHMWPE asperities deform elastically and not plastically (Wang, 2003). In fact, this observation invalidates the hypothesis of a linear relation between the load and the nominal contact area at the basis of the AR law.

Traditionally, the AR and PE wear laws are presented in the following form

$$V = k_{\mathrm{AR}}\ L_{\mathrm{N}}\ s \tag{1}$$

$$V = k_{\mathrm{PE}}\ A\ s \tag{2}$$

where V is the wear volume, k is the wear coefficient, L_{N} the resultant normal load, s the sliding distance and A the nominal contact area. Equations (1) and (2) highlight the main difference between the two wear laws since in the PE law the dependence to the loading conditions is given through the contact area instead of the

normal load. Consequently, the wear coefficients are conceptually different as, k_{AR} is a volume per work unit whilst k_{PE} is a dimensionless quantity.

For complex systems, with contact conditions varying in space and time, the wear laws need to be considered in a local instantaneous form, thus describing the linear wear rate $\dot{h}$ of a surface point P at a generic instant t

$$\dot{h}_{AR}(P,t) = k_{AR}(P,t)\; p(P,t)\,\left|\mathbf{v}(P,t)\right| \tag{3}$$

$$\dot{h}_{PE}(P,t) = k_{PE}(P,t)\,\left|\mathbf{v}(P,t)\right| \tag{4}$$

where $p(P,t)$ is the contact pressure and $\mathbf{v}(P,t)$ is the sliding velocity. This form draws attention to some crucial points. First of all, $\dot{h}_{PE}$ does not depend explicitly on the contact pressure, contrary to $\dot{h}_{AR}$. Secondly, the wear coefficient is not a constant, as considered in many studies (e.g. (Hopkins et al., 2007; Ribeiro et al., 2011)), but, in general, is a function of P and t.

As far as the dependency on time is concerned, the most frequent assumption is the distinction between the initial running-in and the successive steady-state phase. As in this study only the initial wear step is simulated, the dependency on time is not considered, i.e. $k(P)$ instead of $k(P,t)$.

On the other side, several functions of $k(P)$ can be found in the literature specific to UHMWPE, which relate the wear coefficient (AR/PE) to some point dependent feature of the contact surface. Indeed, experimental findings have reported the anisotropic nature of UHMWPE wear, which is affected by multidirectional sliding (Turell et al., 2003; Wang et al., 1997). In particular, the so called cross-shear effect is observed: the polymeric chains assume a principal molecular orientation (*PMO*) so that the wear resistance increases in the *PMO* direction and decreases in the cross-shear direction, which is normal to the *PMO*. In the literature, many different methods have been proposed to quantify the cross-shear, as discussed in (Patten et al., 2014). They are based on the definition of a cross-shear parameter *CS* which is affected by the local operating conditions and thus varying over the plastic surface, i.e. $CS(P)$. In particular, this parameter directly affects the wear factor, resulting in $k(CS) = k(CS(P)) \longrightarrow k(P)$. It is worth noting that the higher the *CS*, the lower the k.

In the present study, the parameter proposed in the first $k_{AR}(CS)$ model presented by (Turell et al., 2003; Wang, 2001) was adopted, which was applied in many numerical wear models of joint prostheses (Kang et al., 2008a; Kang et al., 2009; Liu et al., 2011; Quental et al., 2015). Such a parameter *CS*, also named cross-shear ratio, is defined as the ratio between the total frictional work done perpendicularly to the *PMO* direction and the total frictional work, both considered over a loading cycle with period T. Actually, according to a previous study by the authors (Mattei et al., 2013), the following simplified definition of *CS*, dependent only on the kinematic conditions, was conveniently adopted, which allows the computational cost to be reduced without altering wear indicators:

$$CS(P) = \frac{\int_0^T \left|\mathbf{v}(P,t)\right| \sin^2(\xi(P,t))\; dt}{\int_0^T \left|\mathbf{v}(P,t)\right| dt} \tag{5}$$

where $\xi(P,t)$ is the angle between the sliding velocity and the *PMO* direction. It is worth noting that the *PMO* direction is not known *a priori* and its evaluation requires solving a minimum problem, as it is defined as the direction which minimizes locally the *CS*. According to Eq.(5), the *CS* falls in the range 0–0.5, being 0 in case of unidirectional sliding and 0.5 for circular/squared tracks.

An additional observation on the effect of contact pressure on wear is worth noting. In fact, in some cases k is considered also to depend on contact pressure and, rather counterintuitively, the higher p, the

lower k, as reported by different experimental studies found in the literature (Barbour et al., 1995; Saikko, 2006; Wang et al., 2001). Furthermore, some papers on joint replacements have investigated the coupled influence of the cross-shear and contact pressure on k proposing functions like $k_{AR}(CS, \bar{p})$ with $k_{AR}(CS(P), \bar{p}(P))$, where $\bar{p}(P)$ is the averaged value of $p(P,t)$ over a loading cycle (e.g. (Kang et al., 2009)).

Summing up, according to the Archard wear law three different definitions of k_{AR} were considered in the present wear simulations: a constant value K_{AR}, $k_{AR}(CS)$ from (Wang 2001) and $k_{AR}(CS, \bar{p})$ from (Kang et al., 2009)).

As far as the PE law is concerned, only one type of k is proposed in the literature (Liu et al., 2011) and thus assumed here. Such a wear coefficient depends only on the cross-shear, i.e. $k_{PE}(CS)$, since, according to the PE law (Eqs.(2) and (4)), the contact pressure does not affect the wear rate. In particular, Liu et al. evaluated the wear coefficient as

$$k_{PE}(CS) \approx k_{AR}(CS, \bar{p}) \quad \bar{p} \tag{6}$$

stating that the product on the right side is independent of contact pressure. However, this result is still debated in the literature (Mattei et al., 2013).

2.2.3 Model implementation

The analytical and parametric wear model was implemented in Mathcad®. It has a double function as it can be used both for estimating the wear coefficient k, when experimental measurements are available, and for wear predictions, when k is known. The model was developed for a left RTSA and consisted in a humeral spherical head coupled with a hemispherical glenoid liner or cup (Fig.5-a), the latter fixed into a metal backing. The cup position in the humeral bone was defined by the anteversion and inclination angles, α and β, respectively. Three coordinate systems were introduced, as shown in Fig.5: $S_g=\{O_g, x_g, y_g, z_g\}$ fixed global (x_g: posterior-anterior direction, y_g: medial-lateral direction, z_g: inferior-superior direction), $S_c=\{O_c, x_c, y_c, z_c\}$ fixed on the cup (rotated with respect to Sg according to α and β, and with z_c passing through the cup dome) and $S_h=\{O_h, x_h, y_h, z_h\}$fixed on the head. In the reference configuration, without loading and with head/cup null rotations, S_c and S_h are overlapped and $O_g \equiv O_h \equiv O_c$.

Once the wear law to simulate was defined (i.e. AR or PE law), the data passed as input to the model were:

- Implant geometry: head radius r_h, cup radius r_c (i.e. radius of cup internal surface) and cup thickness t_c, from which radial clearance $cl = r_c - r_h$ and backing radius $r_b = r_c - r_h$
- Cup position: anteversion angle α; inclination angle β
- Material properties: elastic modulus E_c and Poisson coefficient v_c of the cup; irradiation grade of UHMWPE.
- Working conditions: load components and head/cup rotations (angles and rotations sequence) described in S_g and simulating a daily task of period T.
- Wear coefficient/experimental wear volume
- Number of cycles: N_c

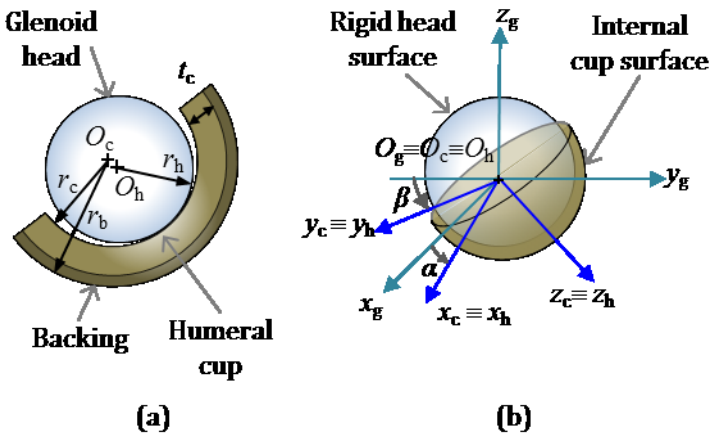

Fig.5. Geometry of RTSA (a) and coordinate frames in the reference configuration with no loading and null rotations (b).

For the present application the following values were assumed:

- r_c= 21.1 mm, *cl*=0.2 mm; t_c=7 mm,
- α =β=0°;
- not cross-linked UHMWPE (0 MRad), E_c =0.5 GPa, ν_c=0.4;
- loading and kinematics conditions used in wear tests (Fig.4)(Kontaxis, 2010);
- wear volume from wear test (see Sec.3.1.): 26.6 mm^3
- N_c = 2 Mc

The model performed the following analyses.

Contact analysis. Firstly, the theoretical contact point on the cup surface was identified by the load vector, which passes through the head and cup centres. Secondly, the contact pressure and area were evaluated according to Bartel's approximated formulas reported in the Appendix A.

Sliding velocity analysis. As underlined in the model hypotheses, only the plastic cup surface is subjected to wear, thus the required sliding velocity in Eqs.(3)-(5) is a component of the relative velocity of a point P_c of the cup surface with respect to the head. This component was evaluated starting from the expressions of the absolute velocity of a generic cup point $P_{c/h}$ of the cup/head surface, as described in the Appendix B.

PMO analysis. The *PMO* direction was evaluated solving an optimization problem, as mentioned above (Eq.(5)).

Wear predictions. The wear depth (or linear wear) in P_c at a given number of wear cycles N_c was estimated by integrating the linear wear rate of Eqs.(3) and (4) over the cycle period T

$$h(P_c) = N_c \int_0^T \dot{h}(P_c, t)\, dt \tag{7}$$

so to obtain the wear map of the plastic cup. The volumetric wear V was then calculated by integrating the wear depth over the contact area A.

$$V = \int_A h(P_c)\, dA \tag{8}$$

2.3 Wear coefficient evaluation

The wear coefficient is a crucial and critical issue in wear predictive modelling, as it affects the model reliability but, at the same time, is hard to estimate. In fact, it depends strictly on all the tribological conditions of a coupling, from geometry to materials, load and kinematics, lubrication and so on. Therefore, although

frequently found in the literature, the use in RTSA wear modelling of k values obtained for other UHMWPE–metal couples like pin-on-disc or hip/knee replacements, should be treated with caution.

In the present study, the described analytical model is also used for evaluating the wear coefficients for a given tribo-system. Such an approach is based on the combination of numerical and experimental wear investigations and takes advantage of the wear coefficient trends available in the literature.

Traditionally, assuming the Archard law and uniform wear, the following expression is used to calculate the constant wear coefficient K_{AR}:

$$K_{\mathrm{AR}} = V^{\exp} / \tilde{V} \tag{9}$$

where $V^{\exp}$ is the experimental wear volume and $\tilde{V}$ the numerical one scaled by the wear coefficient, i.e. the wear volume predicted assuming a unitary wear coefficient.

Unfortunately, when k varies in space and time, Eq.(9) must be revised. The approach followed in this study is based on the fundamental hypothesis that the wear coefficients to be evaluated have trends of *k vs. CS* and *k vs.* $\bar{p}$ similar to those ones reported in the literature for UHMWPE–metal couplings and here denoted as $\hat{k}$. Consequently, the following relation holds

$$k(P,t) = \zeta_{\hat{k}}\, \hat{k}(P,t)\,,\; k = \zeta\, \hat{k} \tag{10}$$

where ζ is an unknown proportionality constant to be determined that depends on both the wear law (AR/PE) and the selected k function, i.e. 1) K_{AR}, 2) $k_{\mathrm{AR}}(CS)$, 3) $k_{\mathrm{AR}}(CS, \bar{p})$ 4) $k_{\mathrm{PE}}(CS)$.

2.3.1 Literature trends

For the Archard constant wear coefficient, reference was made to (Maxian et al., 1997) where $\hat{K}_{\mathrm{AR}} = 1.53\times10^{-6}$ mm^3/(N m). Such a value was estimated by means of experimental and numerical investigations on metal-on-plastic 22 mm diameter hip replacements. In particular, the cups were in GUR415 UHMWPE and were gamma sterilized in ambient air to nominally 2.5 MRad, and the heads were stainless-steel. It should be noted that such $\hat{K}_{\mathrm{AR}}$ was also used in wear simulations of shoulder replacements, both reverse (Quental et al., 2015; Ribeiro et al., 2011) and anatomical, e.g. (Hopkins et al., 2007).

Concerning $\hat{k}_{\mathrm{AR}}(CS)$ the following function in mm^3/(N m) was adopted:

$$\hat{k}_{\mathrm{AR}}(CS) = \begin{cases} (0.328\ln(CS) + 1.62)\,10^{-6} & if\ 0.01 \le CS \le 0.5 \\ 0.1095\times10^{-6} & if\ 0 \le CS \le 0.01 \end{cases} \tag{11}$$

readapted from (Kang et al., 2008a). Indeed, the second equation in (11) provides a threshold value for k, avoiding negative or indefinite values of k for CS<0.008. In particular, Eq.(11) was obtained processing multidirectional pin-on-plate wear tests of not cross-linked (0 MRad) UHMWPE (GUR 1050) pin against Co-Cr plate, under a contact pressure of 1 MPa. Such an expression of k was used in the same study to numerically simulate a wear test on 28 mm total hip arthroplasty in a hip simulator but the predicted wear volume was 31% lower than the experimental (Galvin et al., 2006).

The reference function for $\hat{k}_{\mathrm{AR}}(CS, \bar{p})$ was taken from (Kang et al., 2009) and here readapted for the cases CS<0.01, as similarly done for $\hat{k}_{\mathrm{AR}}(CS)$ in Eq.(11), i.e.

$$\hat{k}_{\mathrm{AR}}(CS, \bar{p}) = \begin{cases} e^{(-13.1+0.19\ln(CS)-0.29\,\bar{p})} & if\ 0.01 \le CS \le 0.5 \\ 0.638\times10^{-6} & if\ 0 \le CS \le 0.01 \end{cases} \tag{12}$$

where the resultant value of k is in mm^3/(N m) and $\bar{p}$ is in MPa. Such a function was based on data from multidirectional pin-on-plate wear tests of UHMWPE-CoCr couplings carried out at several contact pressures. The wear tests are described in different papers by the same research group (1 MPa (Kang et al., 2008a); 3 MPa (Kang et al., 2008b); 6 MPa and 9 MPa (Kang et al., 2009)). Unfortunately, in (Kang et al., 2009) the

irradiation grade of UHMWPE (GUR 1050) is not indicated, though the results suggest the UHMWPE was not cross-linked (i.e. 0 MRad). This wear coefficient function was used to predict wear in hip replacements (Kang et al., 2009) and, as in (Kang et al., 2008a), numerical wear rates underestimated (64% for wear volumes) the corresponding experimental rates (Galvin et al., 2007).

Finally, the following function presented in (Abdelgaied et al., 2011) was assumed for $\hat{k}_{\mathrm{PE}}(CS)$

$$\hat{k}_{\mathrm{PE}}(CS) = (8.5173 \times 10^{-65} + 9.3652 \times 10^{-60}\ CS)^{1/6.7454} \tag{13}$$

It was derived from the multidirectional pin-on-plate wear tests mentioned above (Kang et al., 2008a; Kang et al., 2008b). In particular, wear data obtained at 1 MPa and 3 MPa for not-crosslinked UHMWPE were used to calculate $\hat{k}_{\mathrm{PE}}(CS)$ according to Eq.(6). The wear coefficient of Eq.(13), although applied in wear modelling of knee replacements (Abdelgaied et al., 2011), was preferred to that one used for total hip prostheses presented in (Liu et al., 2011). The main reasons for this are two: i) the lower load levels experienced by TSA with respect to total hip arthroplasty; indeed, in (Liu et al., 2011), $\hat{k}_{\mathrm{PE}}(CS)$ was computed considering only data at 3 MPa that is much higher than the average contact pressure in RTSAs (maximum value below 1 MPa for the simulated conditions); ii) agreement with the wear assumptions for RTSAs in (Quental et al., 2015), thus facilitating the comparison with the literature.

2.3.2 Procedure

The estimation of ζ, and thus of k according to (Eq.(10)), was pursued following four main steps:

1) Experimental wear tests on a given coupling (specific materials and geometry), under given operating conditions, and evaluation of the experimental wear volume (V^{exp}) and maps (h^{exp}).
2) Choice of the wear law/expression among one of the four k functions reported above.
3) Numerical wear simulation of the experimental tests assuming $\zeta = 1$, hence adopting the wear coefficient values/function taken from the literature ($\hat{k}$). Predicted wear volume and depth are denoted as $\hat{V}$ and $\hat{h}$, respectively.
4) Finally, similarly to Eq.(13), the ratio between experimental and numerical wear volumes gives ζ

$$\zeta = V^{\mathrm{exp}} / \hat{V}, \tag{14}$$

from which the wear coefficient can be easily obtained, Eq.(10).

It can be observed that ζ represents a kind of corrective scale factor to be applied to $\hat{k}$ in order to obtain the proper wear coefficient k for the examined tribo-system. It can be noticed that such corrective factor scales linearly both volumes and linear depths, i.e.

$$V = \zeta \hat{V} = V^{\mathrm{exp}} \tag{15}$$

$$h = \zeta \hat{h} \tag{16}$$

As ζ is calculated in order to satisfy the equality of wear volumes (not h), having experimental wear maps (h^{exp}), the following equation could be used to validate wear laws/expressions:

$$h = \zeta \hat{h} = h^{\mathrm{exp}} \tag{17}$$

Unfortunately, due mainly to technological limits/difficulties, experimental wear maps can be found only rarely and for simple geometries. However, their role should be stressed for future advances in wear predictions.

3 Results

3.1 Experimental wear investigations

Over 2 Mc the average polymeric components wear rates were 13.3 ± 1.9 mm^3/Mc. As shown in Fig.6, wear rates were linear, with volume lost increasing in proportion to the number of cycles. To the nearest 0.1mg the control UHMWPE component was unchanged in weight at the end of the 2 Mc test. This compared with a typical weight loss of around 25 mg for test components over the same duration.

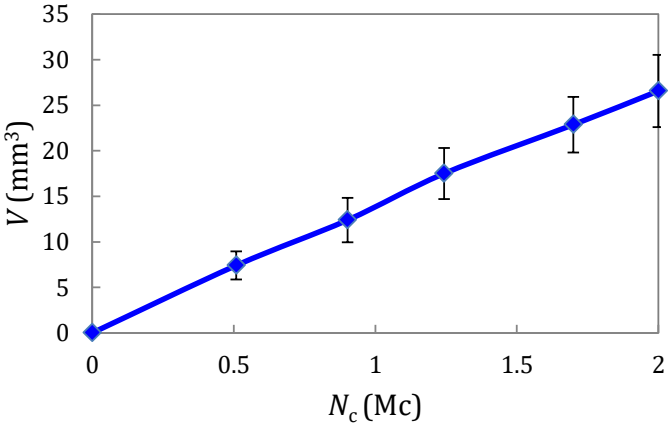

Fig.6. Wear volume of the UHMWPE cups measured in experimental test: A linear increase with the number of cycles was observed.

3.2 Contact and kinematic results

The main results of the contact and kinematic analysis are summarized in Fig.7. Since the load direction was vertical and passing through the cup dome (i.e. fixed with respect to the cup), the contact area resulted always centered with respect to the cup surface (Fig.7a). Accordingly, the maximum contact pressure was located at the cup dome and varies with the load in the range 1.27-1.57 MPa. As far as the kinematic analysis is concerned, both the *CS* and the head/cup relative motion were analyzed. The map of the *CS* of the UHMWPE cup is shown in Fig.7b; it is null outside the contact region while it ranges between 0.06 and 0.22 where contact occurs, with the minimum and maximum values located in diametrically opposed areas. For a deeper comprehension of the *CS* map, the slide tracks of some points of the cup with respect to the head are plotted over the head surface in Fig.7c, i.e. their trajectories are represented in S_h. The selected points P_i are indicated in Fig.7b, and P_1 and P_3 result affected by the highest and lowest *CS* values over the contact area, respectively. Accordingly, P_1 has a quite curly curved trajectory whilst P_3 a narrow and elongated trajectory, which correspond to a more multidirectional and unidirectional sliding motion, respectively. The trajectory of P_4 is quite curved, similarly to that one of P_1, but its *CS* value is lower. Such an effect is attributed to the magnitude of the sliding velocity, which is lower for P_4.

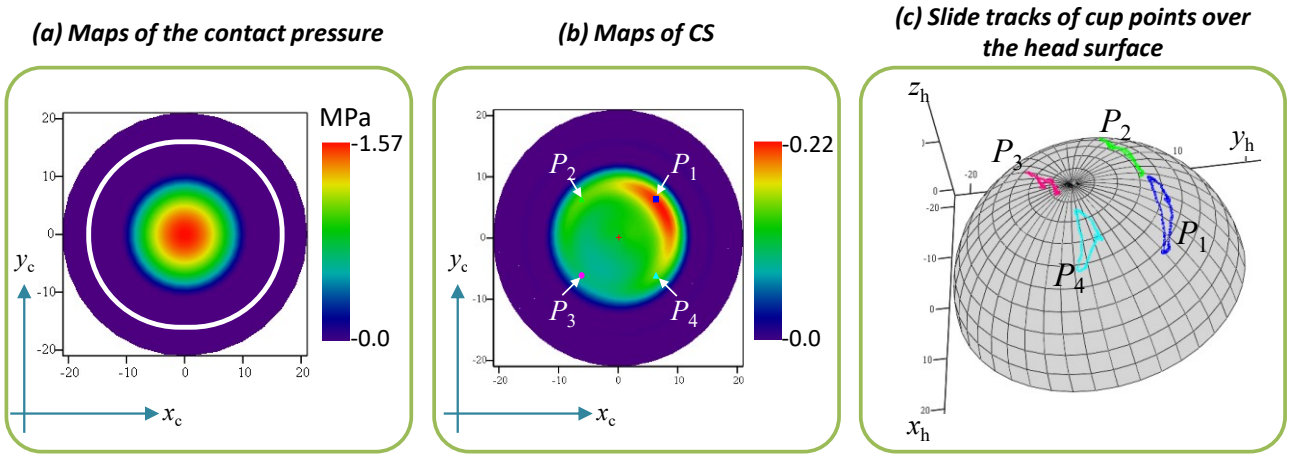

Fig.7. (a) Map of the contact pressure at the maximum load (250 N), on the cup surface in x_c-y_c plane [units of the x_c-y_c axes are in mm]. (b) Map of CS in x_c-y_c plane. [CS is dimensionless]. (c) Slide tracks of the point $P_{1\text{-}4}$ of the cup, also shown in (b), over the head surface (in S_h). Note: The white line in (a) describes the border of the real humeral cup, that is not a complete hemisphere.

3.3 Wear coefficients for RTSAs

One of the main results of the present study is the evaluation of specific wear coefficients for RTSAs, according to the AR and PE laws described above. It is worth stressing that, apart from K_{AR}, all k functions vary from point to point, depending on CS and $k_{AR}(CS, \bar{p})$ also on $\bar{p}$. Thus, in Fig.8, they obtained are plotted over the CS domain ([0–0.5]); for $k_{AR}(CS, \bar{p})$ two curves are depicted in Fig.8.c, for two average contact pressure values, 1 MPa and 3 MPa, as an example. Note also that the wear coefficients k_{AR} for the AR law are dimensional parameters (plotted on the same scale in Fig.8) whilst k_{PE} for the PE law is dimensionless. However, according to Eq.(6), $k_{PE}(CS)$ can be compared to $k_{AR}(CS, \bar{p} = 1 \text{ MPa})\text{x}10^{-3}$.

To ease the comprehension and the discussion, in Fig. 8 the obtained functions of k for RTSAs (in blue) are compared to the $\hat{k}$ taken from the literature (in red) and adopted in Eq.(10). The comparison clearly shows that the functions k and $\hat{k}$ have the same trend, since, according to Eq.(10), k corresponds to $\hat{k}$ scaled by ζ. It can be observed that k and $\hat{k}$ increase with the CS (Fig.8b-d) and decrease with the contact pressure (Fig.8c), as expected from the expressions in Eqs.(11-13). However, the values of the wear coefficient for RTSAs differ significantly from those given in the literature. The RTSA wear coefficients resulted higher than the ones for the hip/knee implants both for the AR and PE law, being $\zeta > 1$ in all considered cases. However, the correction factor for the AR law resulted higher than for the PE law. In particular it was $\zeta = 1.45$ for K_{AR}, $\zeta = 2.41$ for $k_{AR}(CS)$ and $\zeta = 2.20$ for $k_{AR}(CS, \bar{p})$ and $\zeta = 1.32$ for $k_{PE}(CS)$.

Moreover, the scale factor ζ is related to a measure of the error that affects wear predictions for RTSAs when assuming unspecific wear coefficients from the literature, i.e. $\hat{K}_{AR}$ and Eqs.(11)-(13). In particular, it can be assessed that, for the considered case study, the percentage errors in wear predictions assuming $\hat{k}$ instead of k, would be -31%, -58%, -54% and -24% for K_{AR}, $k_{AR}(CS)$, $k_{AR}(CS, \bar{p})$ and $k_{PE}(CS)$, respectively. Such errors could affect RTSA wear studies in the literature: for instance, $\hat{K}_{AR}$ was assumed in (Quental et al., 2015; Ribeiro et al., 2011) and $\hat{k}_{PE}(CS)$ in (Quental et al., 2015).

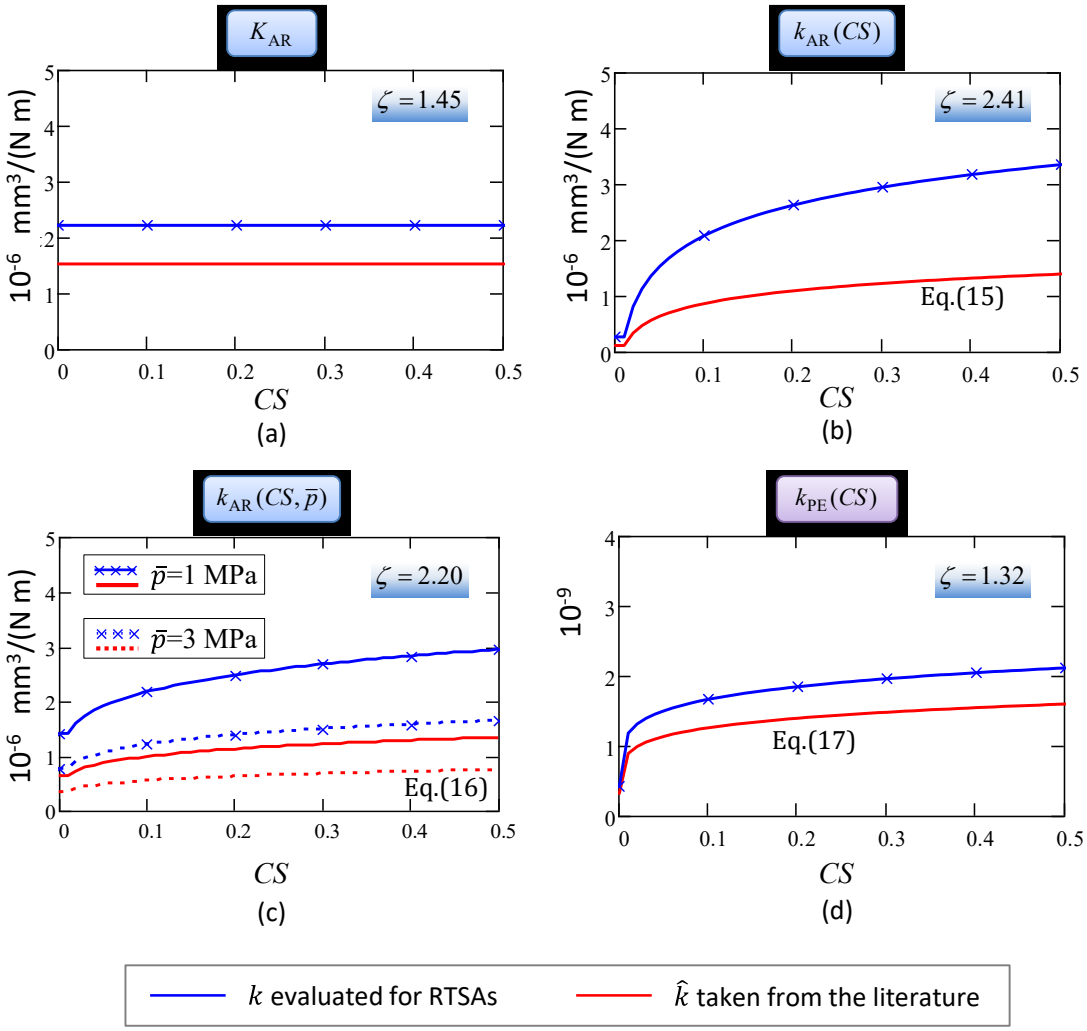

Fig.8. The value/trends of different wear coefficient functions evaluated for RTSAs (k, blue curves) and comparison with the corresponding ones found in the literature ($\hat{k}$, red curves).

3.4 Wear predictions for RTSA with different wear laws

The wear coefficients estimated for RTSAs were then used to numerically simulate the experimental wear test described in Sec.2.1 in order to investigate the influence of different wear laws/coefficients on linear wear predictions. It is worth stressing again that, although all the models estimated the same wear volume (equal to the experimental one), the wear distribution over the articulating surfaces depends on the adopted wear law.

Firstly, the spatial variations of the estimated wear coefficients over the plastic surface were examined. Figures 9a-b show the maps of $k(P)$ for all simulated cases, projected in the x_c-y_c plane (Fig.9c). The maps obtained assuming the AR law and the functions K_{AR}, $k_{AR}(CS)$ and $k_{AR}(CS, \bar{p})$ are plotted respectively in the first three columns of Fig.9. In particular, in Fig.9a the maps are portrayed on different scales, each one within its own minimum and maximum value, whilst, in Fig.9b, they are all reported on the same scale to ease their comparison. The map of k_{PE} is shown on the right of Fig.9d, within its maximum and minimum value. It is worth noting that the definitions of k_{PE} and k_{AR}, as well as their dimensions, are different and thus cannot be directly compared.

The map of K_{AR}, though uniform by definition, is reported for comparative purposes (at the left of Figs.9a and b). The maps of the other k functions, i.e. with $k(P)$, are more informative and reflect the trend of the CS (Fig.7b). Indeed, they were characterized by a uniform value/color outside the contact region (i.e. where CS=0 and $\bar{p}$=0 MPa) and a spatially varying k within the contact region, with the maximum value located

where the maximum *CS* occurred. In particular, the map of $k_{AR}(CS, \bar{p})$ slightly differs from the ones of $k_{AR}(CS)$ and $k_{PE}(CS)$ because of lower values near the cup dome, due to the higher local average contact pressure. From a quantitative point of view, $k_{AR}(CS, \bar{p})$ has a maximum value 16% higher than $k_{AR}(CS)$ (3.2×10^{-6} mm³/(Nm) vs 2.7×10^{-6} mm³/(Nm)), although their average values at the centre of the contact area are similar and about 2×10^{-6} mm³/(Nm) (see the central green areas in the wear maps portrayed on the same scale). It should be noted that the difference between the two k outside the contact area (1.87×10^{-6} mm³/(Nm) vs 0.26×10^{-6} mm³/(Nm), respectively) was due to the effect of $\bar{p}$ on $k_{AR}(CS, \bar{p})$, since $k_{AR}(CS, \bar{p} = 0)$ is higher than $k_{AR}(CS, \bar{p} \neq 0)$. The value of K_{AR}, corresponding to 2.22×10^{-6} mm³/(Nm), though lower than maximum $k_{AR}(CS)$ and $k_{AR}(CS, \bar{p})$, was quite similar to their average value in the centre of the contact region).

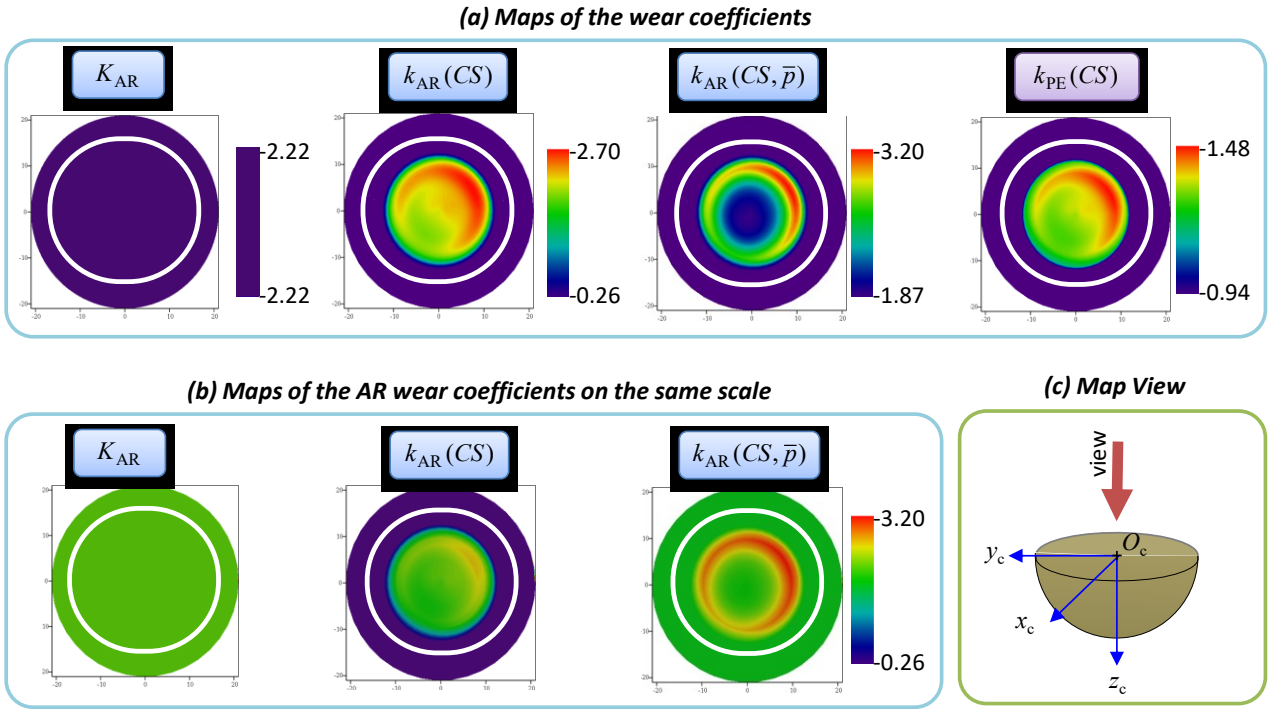

Fig.9. a) Maps of the wear coefficients in x_c-y_c plane. [Values of K_{AR}, $k_{AR}(CS)$ and $k_{AR}(CS, \bar{p})$ are reported in 10^{-6} mm³/(N m), while $k_{PE}(CS)$ is dimensionless but values should be multiplied by 10^{-9}. Units of the x_c-y_c axes are in mm.] b) The maps for the AR wear coefficients in the same scale. c) View direction adopted for plotting the maps. As in Fig.7 the white line describes the border of the real cup.

The wear maps predicted assuming the estimated wear coefficients are plotted (in the x_c-y_c plane) in Fig.10, both on different (Fig.10a) and equal value scales (Fig.10b). All wear maps showed a central worn area, as the load had a fixed direction with respect to the cup, passing through the cup dome.
The wear maps according to the AR law (first three columns of Fig.10) were qualitatively very similar, with the maximum wear depth (h_{max}) located at the cup dome, i.e. where the contact pressure was maximum over all the loading cycle. Differently, the wear map evaluated according to the PE law (last column of Fig.10) presented the maximum wear depth at the inferior and lateral edges of the worn area.

Also in quantitative terms, the results obtained assuming the AR laws were fairly similar to each other, but very different from those ones of the PE law. Indeed, the values of h_{max} estimated adopting K_{AR}, $k_{AR}(CS)$, $k_{AR}(CS, \bar{p})$ were 0.158 mm, 0.156 mm and 0.136 mm, respectively, thus with a maximum percentage difference of about 15%. On the other side h_{max} for $k_{PE}(CS)$ was much lower, 0.105 mm, with the most worn regions located at the edge of the contact area, as discussed above.

The comparison of the wear maps depicted on the same value scale (Fig.10b) highlights well the different wear predictions obtained according to the two wear laws. In particular, lower and more uniform

linear wear was predicted by the PE law with respect to the AR law. These results are in agreement with a previous study on hip implants proposed by the same authors (Mattei et al., 2013).

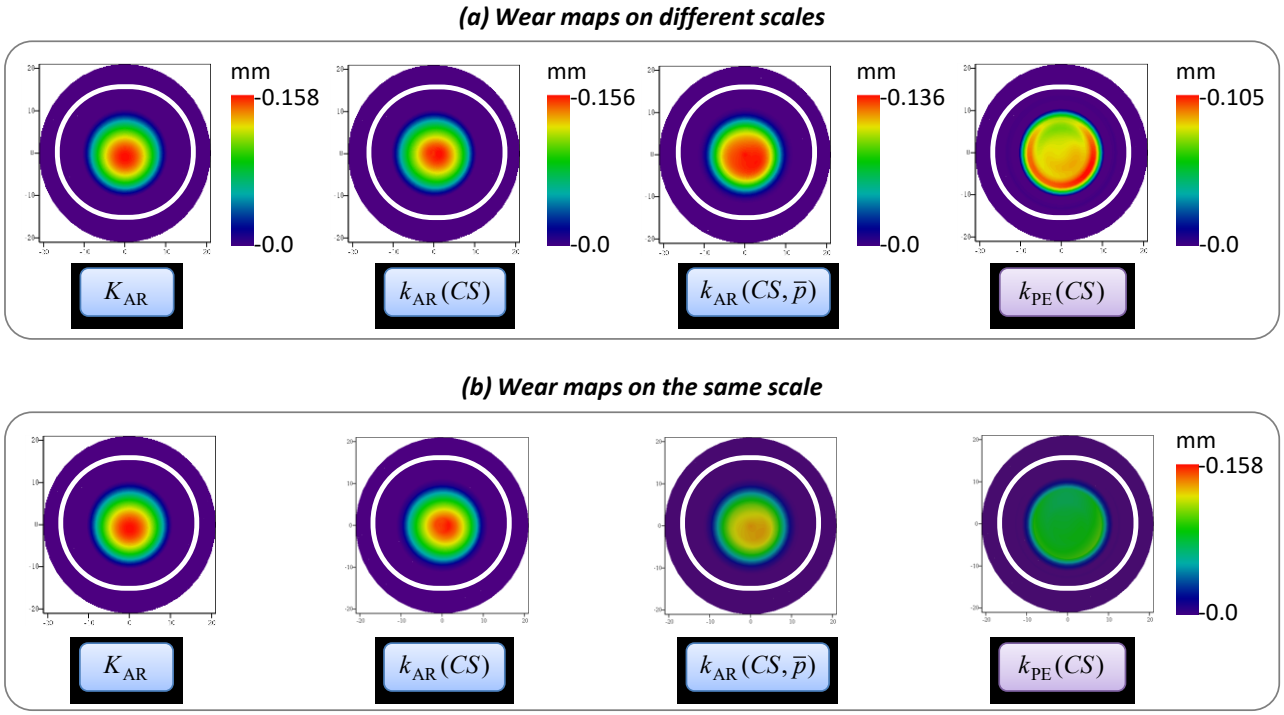

Fig.10. Wear maps of the plastic cup (in x_c-y_c plane) predicted assuming different wear laws (AR/PE) and different k functions. Maps are represented both on different scales, within its minimum and maximum value (a) and the same scale (b). As in Figs.7 and9 the white line describes the border of the real cup.

3.5 Discussion

One important limitation that affects this study derives from the numerical model, which neglects the geometry update due to wear evolution, addressed also in other studies (Mattei and Di Puccio, 2015). Such a hypothesis, although assumed in most wear models of shoulder implants (e.g. (Hopkins et al., 2007; Ribeiro et al., 2011; Terrier et al., 2009)) and holding during the initial phase of the wear process, can affect the reliability of long-term wear predictions (Quental et al., 2015). In particular, according to (Quental et al., 2015), the effect of the geometry update on wear predictions depends on the wear law. For the AR law, specifically for K_{AR}, the wear volume is independent of geometry variation according to (Quental et al., 2015), being related to the frictional work done in a loading cycle (Di Puccio and Mattei, 2015b). This behaviour is in agreement with experimental data reported in Fig.6, showing a linear trend in volume losses. Thus, the obtained K_{AR} wear coefficient can be considered reliable despite model limitations. On the contrary, in the case of the PE law, the wear volume is highly affected by the geometry update. However, it should be considered that the effect of the geometry update is comparable to that of the wear coefficient, so, as a first step towards a more reliable predictive tool, a reliable estimation and the use of couple-specific k are recommended as much as the geometry update.

Another critical point can be seen in the loading conditions applied in the shoulder simulator, as it may initially appear that these are on the low side. However, researchers from other centres have shown comparable values of loading apply to reverse shoulders. For example, Kwon et al (Kwon et al., 2010) and Auckland et al (Ackland et al., 2011) have suggested reverse shoulder joint loads of 10-40% body weight, for an unloaded arm. A computational study by Terrier et al offered similar results for an unloaded arm during abduction, suggesting loads from 110 N to 310 N (Terrier et al., 2008). In a recent cadaveric study, Langohr et al (Langohr et al., 2015) measured glenosphere loads of 250-340 N during abduction. Such loads are different to those reported for total shoulder arthroplasties, see for example Bergman et al (Bergmann et al., 2011). Perhaps this variance should not be surprising giving the very different biomechanical principles

upon which reverse and total shoulders operate. For example, the larger deltoid moment arm in reverse shoulder arthroplasty (Boileau et al., 2005). As another potential limitation, does 'mug to mouth' represent some unusual condition? Human experience would likely indicate this not to be the case, as drinking from cups and other containers is a common activity. In addition it has been shown that such 'mug to mouth' values of loading apply to other common activities of daily living including : reach to opposite axilla; brush opposite side of head; answer telephone; pour from kettle while standing; and lift tray (0.5kg) using both hands (Masjedi and Johnson, 2010).

Finally, a the third limitation involves the actual validation of the model. Presented results describe different wear maps for RTSAs for the same wear volume, i.e. the experimental one (Eqs.(14) and (15)). Thus, in order to validate the wear law and the model, the linear wear should be considered. Unfortunately, as mentioned before, the measure of wear maps, particularly in highly conformal and low wear implants, is very difficult mainly because of technological limits. In particular, to the best knowledge of the authors', experimental wear maps of RTSAs have never been reported in the literature, and rarely even for the more investigated hip implants (Di Puccio and Mattei, 2015b). For the same reasons, to date, the authors are not able to measure h though they are going to address this important issue in future studies. However, some observations of the cup surfaces were made, both by an optical and a scanning electron microscope. In Fig.11 SEM pictures of the new (left) and worn (right) surfaces are compared. Apparently no machining texture is recognizable in the new surface, while the worn images show evident wear tracks. In some cases, deep scratches were observed, possibly produced by wear debris entrapped between the articulating surfaces. Such a type of damage confirms the hypothesis of abrasive wear assumed in wear model formulation and, in particular, in the application of the Archard wear law.

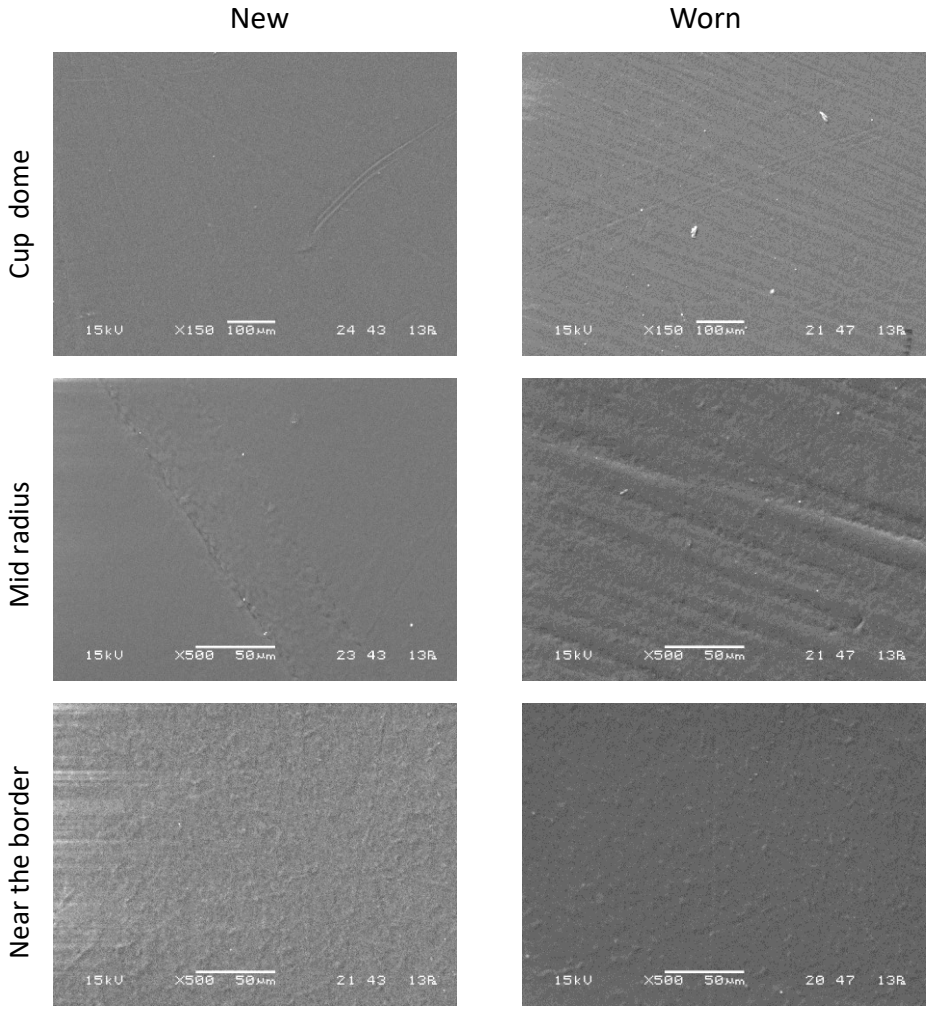

Fig.11 Surface analysis of new (left column) and worn (right column) cups by means of SEM. The worn surface shows evident wear tracks typical of abrasive wear.

Observations at the optical microscope (Fig.12) revealed the initial texture of the surface, with circumferential ridges, which is still is visible in some points of the worn sample, although many scratches are clearly overlaid. Due to the curvatures of the surface, it was hard to find a suitable orientation and position for highlighting the wear damages over the sample surfaces, thus a definite assessment on wear distribution based on these observations would be unreliable. Alternative solution will be investigated.

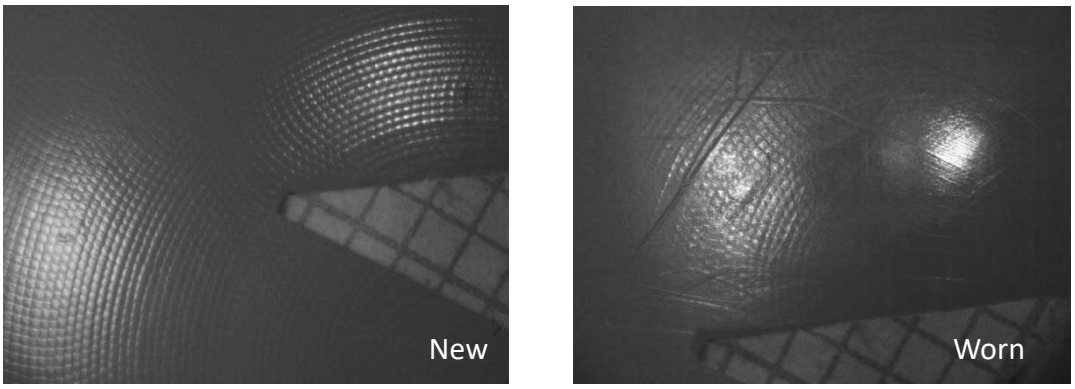

Fig.12 Surface analysis of new and worn cups by means of optical microscope showed typical circumferential ridges due to the manufacturing. In the worn case also many scratches can be observed. A small piece of graph paper (grid 1 mm) was included in the pictures for scaling purposes.

4 Conclusions

In the present study numerical and experimental wear investigations on RTSAs were combined in order to estimate specific wear coefficients for RTSAs. Indeed, none of the few numerical studies on RTSAs available in the literature provide a comparison with wear tests and, especially, they all adopt wear coefficients originally estimated for hip and knee implants (Quental et al., 2015; Ribeiro et al., 2011; Terrier et al., 2009). A wear model previously developed by the authors for metal-on-plastic hip implants was adapted to RTSA cases and applied in a double direction: firstly to evaluate specific wear coefficients for RTSAs (Eqs.(18)) from experimental results, secondly to predict wear distribution. In both cases, the Archard wear law and the wear law of UHMWPE were considered, assuming four different k functions.

Obtained results highlight the remarkable differences between the two wear laws, particularly for the wear distribution. In fact, given the same wear volume, the three versions of the Archard wear law indicate a worn region near the cup dome, with a maximum depth ranging from 0.136 to 0.158 mm. On the other side, according to the PE law, the most worn region is near the border, with a maximum value of 0.105 mm. These differences highlight the necessity of an experimental wear map (not only wear volume) to validate a wear law. Although technical limitations and difficulties are still limiting these measurements, it is important to stress this point as it is rarely considered in the literature for the evaluation of wear laws/wear coefficient functions available, typically estimated using only the wear volume.

Finally, it is worth underlying that, for the Archard wear law, specifically for K_{AR}, the wear volume is independent of geometry variation, thus its estimation is not affected the limitations of the model which does not include the geometry update. In the present case, such law is in agreement with the linearity of the experimental volume loss. Thus, in future models, a value of K_{AR}= 2.22×10^{-6} mm^3/(Nm) could be used and hopefully further verified by wear maps.

References

Abdelgaied, A., Liu, F., Brockett, C., Jennings, L., Fisher, J., Jin, Z., 2011. Computational wear prediction of artificial knee joints based on a new wear law and formulation. J Biomech 44, 1108-1116.

Ackland, D.C., Roshan-Zamir, S., Richardson, M., Pandy, M.G., 2011. Muscle and joint-contact loading at the glenohumeral joint after reverse total shoulder arthroplasty. Journal of Orthopaedic Research 29, 1850-1858.

Barbour, P.S.M., Barton, R.C., Fisher, N., 1995. The influence of contact stress on the wear of UHMWPE for total replacement hip prostheses, 10th International Conference on Wear of Materials, 1 ed. Wear, Switzerland, pp. 250-257.

Bartel, D., Burstein, A., Toda, M., Edwards, D., 1985. The effect of conformity and plastic thickness on contact stresses in metal-backed plastic implants. J Biomech Eng 107, 193-199.

Bergmann, G., Graichen, F., Bender, A., Rohlmann, A., Halder, A., Beier, A., Westerhoff, P., 2011. In vivo gleno-humeral joint loads during forward flexion and abduction. Journal of Biomechanics 44, 1543-1552.

Boileau, P., Watkinson, D.J., Hatzidakis, A.M., Balg, F., 2005. Grammont reverse prosthesis: Design, rationale, and biomechanics. J Shoulder Elbow Surg 14, S147-S161.

Chou, J., Malak, S.F., Anderson, I.A., Astley, T., Poon, P.C., 2009. Biomechanical evaluation of different designs of glenospheres in the SMR reverse total shoulder prosthesis: Range of motion and risk of scapular notching. Journal of Shoulder and Elbow Surgery 18, 354-359.

Brockett, C., Williams, S., Jin, Z., Isaac, G., Fisher, J., 2007. Friction of total hip replacements with different bearings and loading conditions. J Biomed Mater Res B Appl Biomater 81B, 508-515.

Di Puccio, F., Mattei, L., 2015a. Biotribology of artificial hip joints. World J Orthop 6, 77-94.

Di Puccio, F., Mattei, L., 2015b. A novel approach to the estimation and application of the wear coefficient of metal-on-metal hip implants. Tribol Int 83, 69-76.

Farshad, M., Gerber, C., 2010. Reverse total shoulder arthroplasty—from the most to the least common complication. Int Orthop 34, 1075-1082.

Galvin, A., Ingham, E., Fisher, J., 2006. Wear of crosslinked UHMWPE in a hip joint simulator. Journal of Bone & Joint Surgery, British Volume 88-B, 397.

Galvin, A.L., Tipper, J.L., Jennings, L.M., Stone, M.H., Jin, Z.M., Ingham, E., Fisher, J., 2007. Wear and biological activity of highly crosslinked polyethylene in the hip under low serum protein concentrations. Proceedings of the Institution of Mechanical Engineers, Part H: Journal of Engineering in Medicine 221, 1-10.

Hopkins, A.R., Hansen, U.N., Amis, A.A., Knight, L., Taylor, M., Levy, O., Copeland, S.A., 2007. Wear in the prosthetic shoulder: association with design parameters. J Biomech Eng 129, 223-230.

Kang, L., Galvin, A.L., Brown, T.D., Fisher, J., Jin, Z.M., 2008a. Wear simulation of ultra-high molecular weight polyethylene hip implants by incorporating the effects of cross-shear and contact pressure. Proceedings of the Institution of Mechanical Engineers, Part H (Journal of Engineering in Medicine) 222, 1049-1064.

Kang, L., Galvin, A.L., Brown, T.D., Jin, Z., Fisher, J., 2008b. Quantification of the effect of cross-shear on the wear of conventional and highly cross-linked UHMWPE. J Biomech 41, 340-346.

Kang, L., Galvin, A.L., Fisher, J., Jin, Z., 2009. Enhanced computational prediction of polyethylene wear in hip joints by incorporating cross-shear and contact pressure in additional to load and sliding distance: Effect of head diameter. J Biomech 42, 912-918.

Kohut, G., Dallmann, F., Irlenbusch, U., 2012. Wear-induced loss of mass in reversed total shoulder arthroplasty with conventional and inverted bearing materials. J Biomech 45, 469-473.

Kontaxis, A., 2010. Biomechanical analysis of reverse anatomy shoulder prosthesis. Newcastle University.

Kwon, Y.W., Forman, R.E., Walker, P.S., Zuckerman, J.D., 2010. Analysis of Reverse Total Shoulder Joint Forces and Glenoid Fixation. Bulletin of the NYU Hospital for Joint Diseases 68, 273–280.

Langohr, G.D.G., Giles, J.W., Athwal, G.S., Johnson, J.A., 2015. The effect of glenosphere diameter in reverse shoulder arthroplasty on muscle force, joint load, and range of motion. Journal of Shoulder and Elbow Surgery 24, 972-979.

Liu, F., Galvin, A., Jin, Z., Fisher, J., 2011. A new formulation for the prediction of polyethylene wear in artificial hip joints. Proceedings of the Institution of Mechanical Engineers, Part H: Journal of Engineering in Medicine 225, 16-24.

Liu, F., Jin, Z.M., Grigoris, P., Hirt, F., Rieker, C., 2003. Contact mechanics of metal-on-metal hip implants employing a metallic cup with a UHMWPE backing. Proceedings of the Institution of Mechanical Engineers, Part H: Journal of Engineering in Medicine 217, 207-213.

Masjedi, M., Johnson, G.R., 2010. Glenohumeral contact forces in reversed anatomy shoulder replacement. Journal of Biomechanics 43, 2493-2500.

Mattei, L., Di Puccio, F., 2015. Influence of the wear partition factor on wear evolution modelling of sliding surfaces. International Journal of Mechanical Science 99, 72-88.

Mattei, L., Di Puccio, F., Ciulli, E., 2013. A comparative study on wear laws for soft-on-hard hip implants using a mathematical wear model. Tribol Int 63, 66-77.

Maxian, T., Brown, T., Pedersen, D., McKellop, H., Lu, B., Callaghan, J., 1997. Finite element analysis of acetabular wear. Validation, and fixation and backing effects. Clin Orthop Relat Res 344, 111-117.

Nam, D., Kepler, C.K., Neviaser, A.S., Jones, K.J., Wright, T.M., Craig, E.V., Warren, R.F., 2010. Reverse Total Shoulder Arthroplasty: Current Concepts, Results, and Component Wear Analysis. The Journal of Bone & Joint Surgery 92, 23-35.
Nyffeler, R.W., Werner, C.M.L., Simmen, B.R., Gerber, C., 2004. Analysis of a retrieved Delta III total shoulder prosthesis. Journal of Bone and Joint Surgery Br 86-B, 1187-1191.
Patten, E.W., Van Citters, D., Ries, M.D., Pruitt, L.A., 2014. Quantifying cross-shear under translation, rolling, and rotation, and its effect on UHMWPE wear. Wear 313, 125-134.
Peers, S., Moravek, J.E., Jr., Budge, M.D., Newton, M.D., Kurdziel, M.D., Baker, K.C., Wiater, J.M., 2015. Wear rates of highly cross-linked polyethylene humeral liners subjected to alternating cycles of glenohumeral flexion and abduction. J Shoulder Elbow Surg 24, 143-149.
Quental, C., Folgado, J., Fernandes, P.R., Monteiro, J., 2015. Computational analysis of polyethylene wear in anatomical and reverse shoulder prostheses. Med Biol Eng Comput 53, 111-122.
Ribeiro, N.S., Folgado, J., Fernandes, P.R., Monteiro, J., 2011. Wear analysis in anatomical and reversed shoulder prostheses. Comput Methods Biomech Biomed Engin 14, 883-892.
Saikko, V., 2006. Effect of contact pressure on wear and friction of ultra-high molecular weight polyethylene in multidirectional sliding. Proc Inst Mech Eng H 220, 723-731.
Smith, S., Li, B.L., Buniya, A., Ho Lin, S., Scholes, S.C., Johnson, G., Joyce, T.J., 2015. In vitro wear testing of a contemporary design of reverse shoulder prosthesis. J Biomech, BMD1500176. http://dx.doi.org/10.1016/j.jbiomech.2015.07.022.
Smith, S., Li, L., Johnson, G., Joyce, T., 2013. First wear results from a unique multi-station shoulder joint simulator, 5th World Tribology Congress, WTC 2013, pp. 407-408.
Terrier, A., Reist, A., Merlini, F., Farron, A., 2008. Simulated joint and muscle forces in reversed and anatomic shoulder prostheses. J Bone Joint Surg Br 90-B, 751-756.
Terrier, A., Merlini, F., Pioletti, D.P., Farron, A., 2009. Comparison of polyethylene wear in anatomical and reversed shoulder prostheses. Journal of Bone & Joint Surgery, British Volume 91-B, 977-982.
Turell, M., Wang, A., Bellare, A., 2003. Quantification of the effect of cross-path motion on the wear rate of ultra-high molecular weight polyethylene. Wear 255, 1034-1039.
Vaupel, Z.M., Baker, K.C., Kurdziel, M.D., Wiater, J.M., 2012. Wear simulation of reverse total shoulder arthroplasty systems: effect of glenosphere design. J Shoulder Elbow Surg 21, 1422-1429.
Wang, A., 2001. A unified theory of wear for ultra-high molecular weight polyethylene in multi-directional sliding. Wear 248, 38-47.
Wang, A., Essner, A., Klein, R., 2001. Effect of contact stress on friction and wear of ultra-high molecular weight polyethylene in total hip replacement. Proceedings of the Institution of Mechanical Engineers, Part H: Journal of Engineering in Medicine 215, 133-139.
Wang, A., Sun, D.C., Yau, S.S., Edwards, B., Sokol, M., Essner, A., Polineni, V.K., Stark, C., Dumbleton, J.H., 1997. Orientation softening in the deformation and wear of ultra-high molecular weight polyethylene. Wear 203-204, 230-241.
Wang, F.C., 2003. Microscopic asperity contact and deformation of ultrahigh molecular weight polyethylene bearing surfaces. Proc Inst Mech Eng H J Eng Med 217, 477-490.
Wiater, B.P., Moravek Jr, J.E., Wiater, J.M., 2014. The evaluation of the failed shoulder arthroplasty. J Shoulder Elbow Surg 23, 745-758.

Appendix A: Contact analysis

In the present study, the contact problem was solved by means the approximated formulas for the contact pressure and the contact area of metal-backed on plastic implants with ball-in-socket geometry proposed in (Bartel et al., 1985). Such formulas were obtained moving from equilibrium equations and geometrical observations. Indeed, considering the head being rigid, the cup deformed geometry is fully known. In particular, with the exception of edge-loading cases, the contact stress/strain conditions are symmetric with respect to the loading axis marked in red in Fig.A1. The following hypotheses are worth reminding

1. The head is considered rigid with respect to the cup.
2. The circumferential components of the cup elastic deformation are negligible with respect to the radial one.

3. The derivatives of all elastic displacement components with respect to the circumferential directions are negligible.
4. The direction normal to the contact is defined with respect to the undeformed configuration, i.e. passing through the cup centre.

Thus, as the load is applied, it causes a radial displacement of the cup surface δ, which decreases with the angular distance θ from the loading axis and ranges from a maximum value Δ at θ=0°and a null value at the edge contact.

The unknown contact variables, depending on the loading conditions, are: $\Delta(t)$, $\delta(P_c t)$ and the contact pressure $p(P_c, t)$, with P_c being a point of the cup surface. However, on the basis of the considerations above and omitting the time-dependence, they can be written as Δ, $\delta(\theta)$ and $p(\theta)$.

Such variables can be found solving numerically, at every instant t, the following equations system.

1. The equilibrium equations written in spherical coordinates (r, θ, φ) on the basis of hypotheses 2 and 3 are combined to the generalized Hooke law for obtaining a single differential equation with only the radial displacement $u_r(r, \theta, \varphi)$. Moreover, considering the symmetry of the problem, it results $u_r(r, \theta)$. The latter is solved assuming as working conditions $u_r(r_b, \theta)=0$, the metal backing being rigid compared to the plastic cup, and $u_r(r_c, \theta)=\delta(\theta)$. The radial stress at the internal cup surface, i.e. the contact pressure, is so obtained

$$p(\theta)=\left(\frac{1}{1-2\nu}+\frac{2}{1+\nu}\frac{1}{(r_c/r_b)^3}\right)\frac{E}{(r_c/r_b)^3-1}\frac{\delta(\theta)}{r_c} \tag{A.1}$$

2. The cosine law is applied to the triangle $\breve{P}_c O_c O_h$, with $\breve{P}_c$ corresponding to the cup surface point P_c in the deformed configuration, and gives a 2° order equation in $(r_c+ u_r(r_c, \theta))$, whose solution leads to

$$\delta(\theta)=\left(\cos(\theta)+\sqrt{\left(\frac{r_h}{r_c-r_h+\Delta}\right)^2-\sin^2(\theta)}\right)\left(r_c-r_h+\Delta\right)-r_c \tag{A.2}$$

It is worth noting that imposing $\delta(\theta_{max})=0$, Eq.(A.2) provides

$$\theta_{max}=\cos^{-1}\left(\frac{r_c^2-r_h^2+(r_c-r_h+\Delta)^2}{2\,r_c\,(r_c-r_h+\Delta)}\right) \tag{A.3}$$

3. The equilibrium between the contact pressure and the load **L** at every instant t, is written according to hypothesis 9, i.e. considering the direction normal to the contact along $\breve{P}_c O_c$

$$L=\pi\int_0^{\theta_{max}} p(\theta)\;(r_c+\delta(\theta))^2\,\sin(2\theta)\,d\theta \tag{A.4}$$

It should be noted that, in the present study the elastic deformation is neglected in the kinematic analysis, thus approximating $\breve{P}_c$ to P_c.

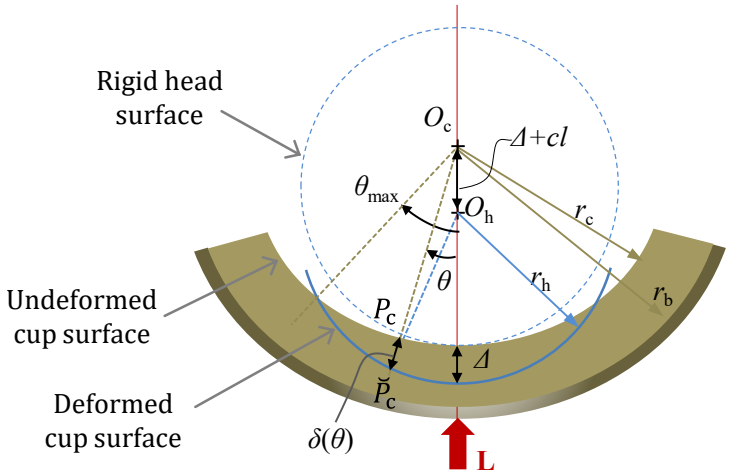

Fig.A1. RTSA in contact configuration: the rigid head indents the elastic cup causing a maximum radial deflection of Δ along the loading axis.

Appendix B: sliding velocity

According to the well-known expressions of the differential kinematics of a rigid body, the absolute velocity of a generic cup point $P_{c/h}$ on the cup/head surface can be written as

$$\mathbf{v}_{P_c} = \mathbf{v}_{O_c} + \omega_c \times O_c P_c \tag{B.1}$$

$$\mathbf{v}_{P_h} = \mathbf{v}_{O_h} + \omega_h \times O_h P_h \tag{B.2}$$

where $\omega_{c/h}$ are the cup/head angular velocities. Note that the velocity of a point P, i.e. $\mathbf{v}(P,t)$, is written as $\mathbf{v}_P$ and all time-dependences are omitted per simplicity. As the head centre O_h is considered fixed, the relative velocity of the cup point P_c with respect to the head is given by

$$\mathbf{v}^r = \mathbf{v}_{O_c} + \omega_c \times O_c P_c - \omega_h \times O_h P_c \tag{B.3}$$

The cup sliding velocity $\mathbf{v}^s$, is the component of the relative velocity lying in the plane tangent to the cup surface at P_c

$$\mathbf{v}^s = \mathbf{v}^r - \frac{(\mathbf{v}^s \cdot O_c P_c)\, O_c P_c}{r_c^2} \tag{B.4}$$